Supplementary Information

Photosensitizer and Vancomycin-conjugated Novel Multi-functional Magnetic Particles as Photoinactivation Agent for Selective Killing of Pathogenic Bacteria

Kyong-Hoon Choi[a,1], Hye-Jin Lee[b,1], Bong Joo Park[a,1], Kang-Kyun Wang[a], Eon Pil Shin[a], Jong-Chul Park[c], Young Keun Kim[d], Min-Kyu Oh[b,*], Yong-Rok Kim[a,*]

[a]Photon Applied Functional Molecule Research Laboratory, Department of Chemistry, Yonsei University, Seoul 120-749, Republic of Korea

[b]Systems Bioengineering Laboratory, Department of Chemical & Biological Engineering, Korea University, Seoul 136-701, Republic of Korea

[c]Department of Medical Engineering, Yonsei University College of Medicine, Seoul 120-752, Republic of Korea

[d]Department of Materials Science and Engineering, Korea University, Seoul 136-713, Republic of Korea

[1] These authors contributed equally to this work.

I: Experimental Section

Preparation of the Fe_3O_4 particles The Fe_3O_4 submicron particles were fabricated using a solvothermal reduction method reported previously.[1] $FeCl_3 \cdot 6H_2O$ (1.35 g, 5 mmol) and polyethylene glycol (1.0 g) were dissolved in ethylene glycol (40 mL) to form a clear solution, and then NaAc (3.6 g) was added into the mixture under vigorous stirring condition for 30 min. As-formed viscous slurry was transferred into a teflon-lined stainless-steel autoclave of 80 mL capacity. The autoclave was heated to and maintained at 200 °C for 8 h, and naturally cooled to room temperature. The obtained black precipitates were collected after being washed with distilled water and absolute alcohol several times and dried at 60 °C for 6 h.

Photosensitizer and vancomycin conjugation to Fe_3O_4 particles The Fe_3O_4@t-PtCP particles were prepared by wet chemical process with [5,15-bisphenyl-10,20-bis(4-methoxycarbonylphenyl)-porphyrin] platinum (t-PtCP) as follows. The t-PtCP molecules were synthesized as previously described.[2] The Fe_3O_4 particles in THF (30 mg / mL, 5 mL THF) were mixed with the solution of the t-PtCP (5×10^{-2} mM, 5 mL THF). The mixture was agitated at room temperature for 24 h. After the reaction was complete, the product was washed with THF solvent several times. After the final washing, the residual THF solvent was further removed and then dried at 60 °C for 6 h. The collected 1 mg of Fe_3O_4@t-PtCP particles were then transferred into a vial containing 1 mL of the PBS solution (138 mM NaCl, 2.7 mM KCl, 5.4 mM Na_2HPO_4, 1.8 mM KH_2PO_4, pH 7.4). The PBS solution was vortexed for washing. After washing, the residual PBS solution was removed and then Fe_3O_4@t-PtCP particles were resuspended in 1 mL of new PBS solution to achieve 1 mg/mL concentration (about 2.37×10^{10} particles/mL).

The solution of Fe_3O_4@t-PtCP particles (1 mg/mL) was mixed with VAN solution (1 mg/mL) and N-(3-dimethylaminopropyl)-N'-ethylcarbodiimide hydrochloride (EDAC)

aqueous solution (1 mg/mL).[3] The mixture solution was stirred at 4 °C under mild shaking condition (50 rpm) during 24 h of incubation. After the reaction, the solution was placed on a magnet for 1 min and any unbound VAN in the supernatant was removed to another vial. The VAN conjugated Fe_3O_4@t-PtCP particles (MMPs) were washed three times with the PBS solution and incubated with 1 mL Tris·HCl buffer (50 mM, pH 7.4) under the shaking condition of 200 rpm for 30 min.

Characterization of the MMPs Transmission electron microscopy (TEM, JEOL, JEM-2100F) and field emission scanning electron microscopy (FE-SEM, Hitachi, SU-70) were utilized to study the morphology of the MMPs. Crystallographic structure of the composite particle was investigated with a X-ray diffractometer (XRD, PANalytical, X` Pert Pro MPD) working on Cu Kα radiation. A vibrating sample magnetometry (VSM, Lakeshore 7300) was used to obtain the magnetization versus magnetic field loop up to H = 10 kOe at room temperature. Infrared spectra were obtained by using a PerkinElmer FT-IR (spectrum 100 spectrometer). For IR measurements, the samples were crushed in an agate mortar and then prepared as the pressed wafers (ca. 1 wt % sample in KBr). Absorption and emission spectra were obtained with a diffuse reflectance UV-Vis spectrophotometer (Jasco V-550) equipped with an integrating sphere (Jasco ISV-469) and a spectrofluorometer (Hitachi, F-4500), respectively.

Detection of singlet oxygen In order to get the relative $^1O_2$ quantum yield of the multifunctional magnetic particles in comparison with that of the t-PtCP molecule, the $^1O_2$ lifetime measurements for both samples were performed with the THF solutions due to the solubility of the samples in THF. Generation of singlet oxygen ($^1O_2$) and its relaxation lifetime were detected by the characteristic phosphorescence emission peak at 1270 nm.[4]

Optical parametric oscillator (OPO) laser (B.M. Industries OP901-355, 5 ns FWHM pulse) pumped by Nd-YAG (BMI series, 7 ns FWHM pulse) was utilized as an excitation source. Phosphorescence signal was collected at the perpendicular angle to the excitation beam and detected with a monochromator (Optometrics LLC, mini-chrom04) and NIR-PMT (Hamamatsu, H9170-45). The signal was acquired by 500 MHz digital oscilloscope (Hewlett Packard, 54520A) and transferred to a computer for data analysis.

Diffusion distance of singlet oxygen in aqueous solution If we restrict ourselves to the case in which the diffusion is radial, then the distance, d, that is traveled by singlet oxygen can be expressed in the following equation, using the Stokes-Einstein relation:[5]

$$d = \sqrt{6tD}$$

where t and D are the radial diffusion time period (i.e. singlet oxygen lifetime) and the singlet oxygen diffusion coefficient in water, respectively.

The diffusion coefficient, D, for singlet oxygen in water is 2×10^{-5} cm^2s^{-1},[6] and the general singlet oxygen lifetime in water is ~ 4 μs.[7] Based on these factors, the estimated distance traveled by singlet oxygen in water is ~ 219 nm until 63 % of the generated singlet oxygen population disappears. The kinetic lifetime defines the period in which a given population is reduced by a factor of 1/e. Therefore, there is still an appreciable population of singlet oxygen remaining, and the singlet oxygen residues will continue to diffuse throughout the surrounding medium.

Photodynamic killing of pathogenic bacteria Four Gram-positive bacteria (*E. faecalis* (ATCC 19433), *S. aureus* (KCCM 40253), *B. cereus* (KCCM 40935), and MSSA (ATCC 29213)) and two Gram-negative bacteria (*E. coli* O157:H7:K^- (ATCC 700927) and *S.*

typhimurium (IFO 14193)) were acquired from strain banks. Clinical isolates of two Gram-positive bacteria (MRSA and VRE) were donated from a hospital at Korea University. These strains were grown in Brain Heart Infusion (BHI) medium. The bacteria were cultured at 37 °C for 15 h. Then, the culture media were centrifuged and bacteria were washed with PBS solution. Bacteria concentrations were determined with UV-Vis spectrophotometer and confirmed by spreading bacteria on either BHI agar plate or BAP (Blood Agar plate) and incubating them at 37 °C for 15 h, followed by colony counting. The volume of PBS solution was adjusted to achieve a target concentration of cells, 10^6 CFU/mL. For capturing bacteria, the MMPs were mixed with bacteria solution. The mixture was incubated at room temperature under shaking (150 rpm) for 2 h. Then, the bacteria captured by the MMPs were collected by a magnet and the supernatant was removed into a new vial for calculating capture efficiency. Bacteria and the MMPs complexes were washed five times with PBS solution and resuspended in 1 mL PBS solution. Then they were spreaded on BHI agar plate or BAP for counting the number of bacteria in capture fraction. Next, to examine the killing of bacteria, the bacteria captured MMPs complex were irradiated by a laser at various time intervals. The Nd-YAG pumped OPO laser with a wavelength of λ=510 nm and a pulse width of 7 ns was irradiated into a spot area of about 1.23 cm^2. The laser energy density was 6.1 $mWcm^{-2}$ with a repetition rate of 10 Hz. After irradiation, the complexes of the bacteria captured MMPs were spread on a BHI agar plate or BAP and incubated at 37 °C for 15 h in order to estimate the survival percentage of bacteria. Each experiment was duplicated.

Cytotoxicity assessment of the MMPs Cytotoxicity of MMPs itself on mammalian cells is essential to evaluate the potential for bio and clinical applications of MMPs. As described by the document of International standard ISO 10993-5,[8] cytotoxicity test using the L-929, mouse fibroblast cells, (ATCC CCL 1, NCTC Clone 929, of strain L) cells was performed as

follows: pre-cultured cells were plated in 24-well plate at 1.0×10^5 cells per well and incubated at 37°C for 24 hrs in order to obtain confluent monolayer's of cells prior to use. After 24 hrs, all cultures were treated with various concentrations (0, 75, 150, 300, 600 μg/mL) of MMPs and incubated for 24 hrs, under the same growth conditions. The plates were washed three times with PBS solution after incubation. Each culture was stained with MTT solution and lysed with DMSO solution. The absorbance of each well was measured at 570 nm with an automatic microplate reader (Spectra Max 340, Molecular Device Inc., Sunnyvale, CA., USA). The relative cell viability was expressed as a percentage of the optical densities of the MMPs treated samples to the optical densities of the samples grown in the control medium.

II. Supplementary Figures and Discussions

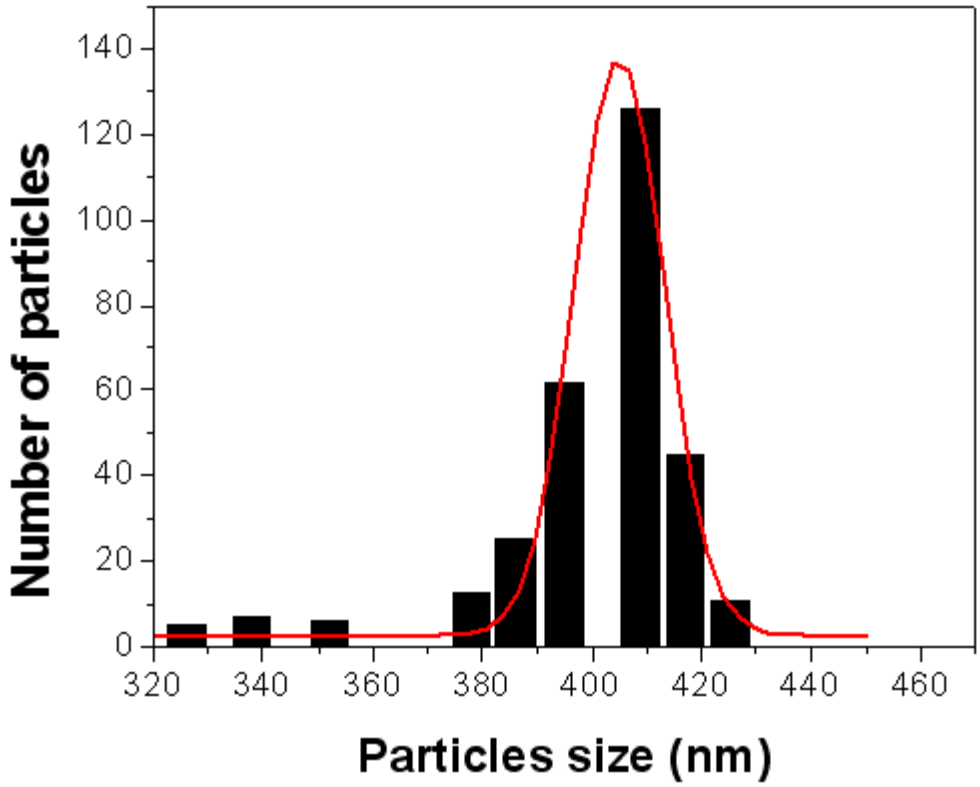

Fig. S1. The histogram for the particle size distribution of pure Fe_3O_4 submicron particles.

The size histogram of the Fe_3O_4 particles estimated by sampling 300 particles in different regions of the FE-SEM image. It indicates that the particles have a good size uniformity and the average particle size is 400 nm with a distribution of ± 19 nm.

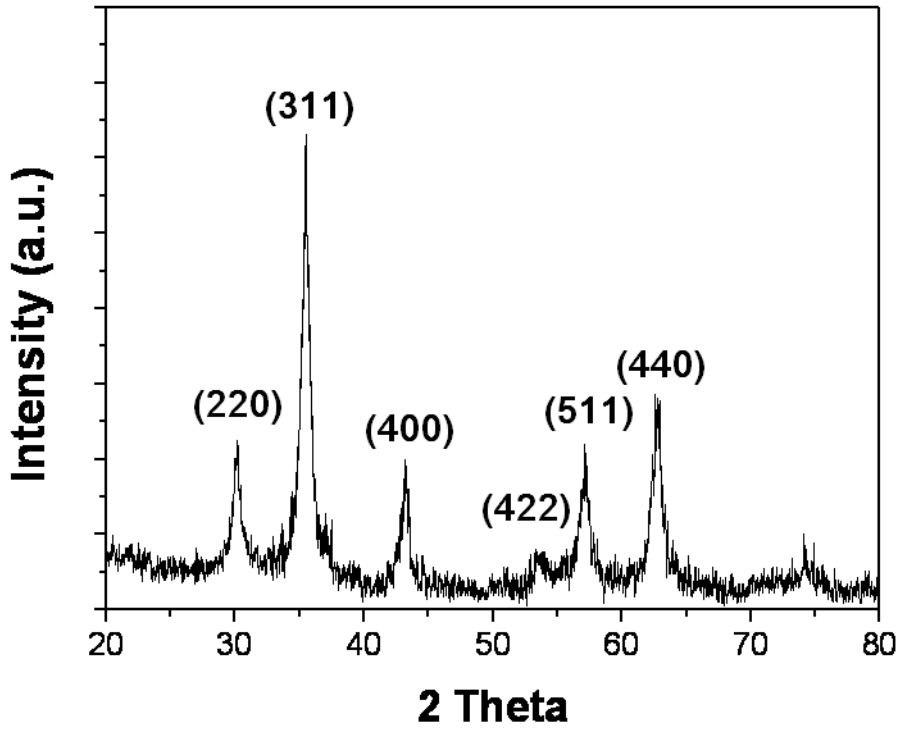

Fig. S2. The XRD pattern of the Fe_3O_4 particles.

The powder XRD pattern of the Fe_3O_4 particle provides more detailed structural information, as shown in Fig. S2. The strong Bragg reflection peaks (2 = 30.0, 35.6, 43.3, 53.7, 57.0, 62.8°) are marked by their Miller indices ((220), (311), (400), (422), (511), and (440)) that are obtained from the standard Fe_3O_4 powder diffraction data (JCPDS, card 19-0629). The position and relative intensity of all diffraction peaks match well with the characteristic peaks of the magnetite crystal with cubic inverse spinel structure. The average particle diameter is estimated from the Debye–Scherrer equation to be about 13 nm, which is in close agreement with the FE-SEM results for the small nanoparticles, the aggregated form of which results in the big particle of 400 nm.

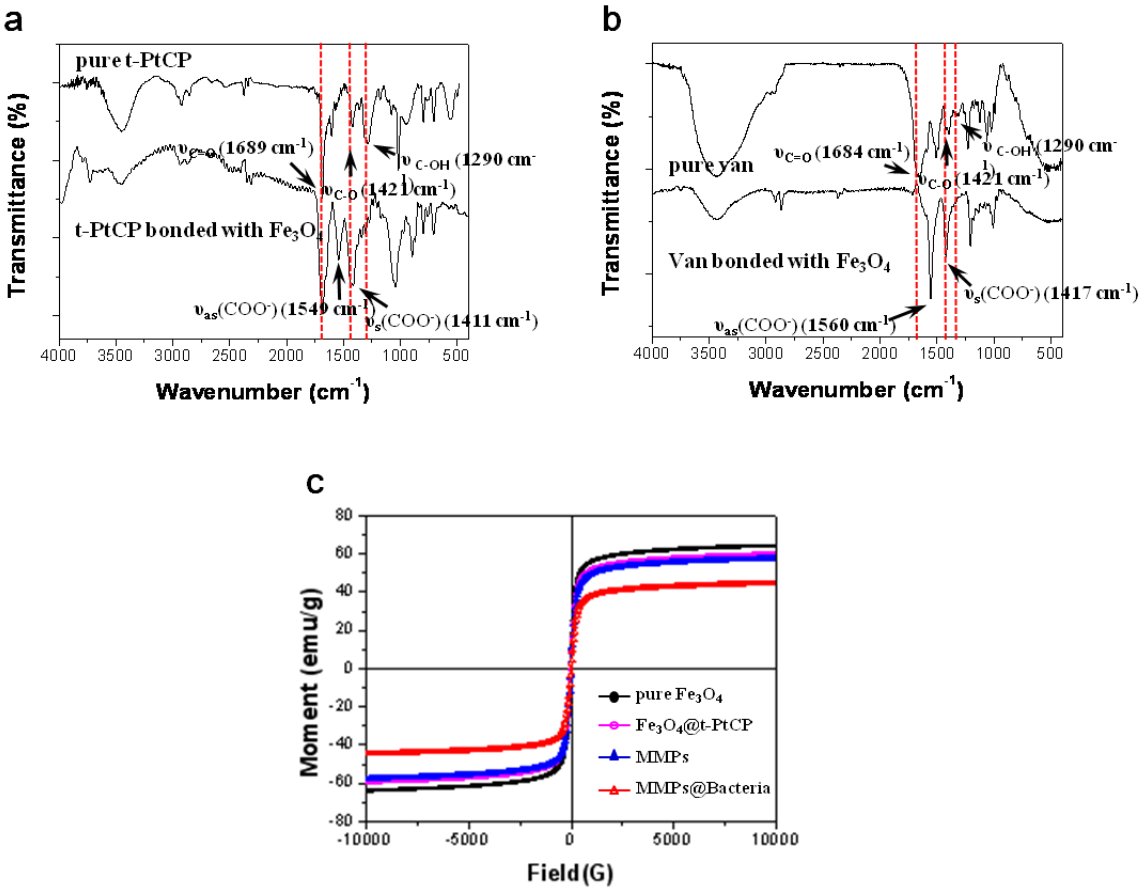

Fig. S3. FT-IR spectra of: (a) pure t-PtCP and t-PtCP bonded with Fe_3O_4; (b) pure VAN and VAN bonded with Fe_3O_4; (c) room-temperature magnetic hysteresis loops of the MMPs in the step-by-step fabrication process.

As reported previously,[9] the IR spectrum of pure t-PtCP presents the absorption peaks at 1689 cm^{-1}, 1421 cm^{-1}, and 1290 cm^{-1}, which correspond to the stretching modes of the free carbonyl double bond ($\upsilon_{C=O}$), the carbon-oxygen single bond (υ_{C-O}), and the O-H deformation (υ_{C-OH}), respectively (Fig. S3a). These characteristic absorption peaks suggest that pure t-PtCP has protonated carboxyl groups (COOH), as expected. After the conjugation reaction occurs between the carboxyl group and the Fe ion, the IR spectrum of the t-PtCP bonded to Fe_3O_4 presents the peaks corresponding to the protonated carboxyl group and, in addition, the new bands appear at 1549 cm^{-1} and 1411 cm^{-1}, which are ascribed to the asymmetric (υ_{as}) and

the symmetric (υ_s) stretch vibrations of the carboxylate group, respectively. The appearance of these new bands is in agreement with the results of the IR bands reported by Dravid et al.[10] They suggested that the IR bands at 1556 cm^{-1} and 1410 cm^{-1} corresponded to the υ_{as} and the υ_s stretching modes of the carboxylate in their oleic acid system, which showed coordination bonding between the carboxylate and the cobalt ion on the surface of the cobalt nanoparticle. The spectrum shows that the protonated carboxyl group substantially disappears and the new bands appear at 1560 cm^{-1} and 1417 cm^{-1} (Fig. S3b). Such a pattern of spectral change is also attributed to the formation of Fe-carboxylate complexation due to chemical coordination, as in the previous case.

Fig. S3c shows the change in the saturation magnetization for the various samples obtained during the step-by-step surface modification process of the MMPs. The magnetization curves of all the samples exhibited no hysteresis and no coercivity even with a high magnetic field, indicating that all submicron particles are superparamagnetic. As observed in the FE-SEM images and X-ray diffraction pattern, the Fe_3O_4 particles are composed of many small nanoparticles, 15~20 nm in diameter. Therefore, this superparamagnetic behavior is attributed to the small nanoparticles, with a diameter less than 20 nm, which aggregate to the submicron sphere. This result agrees well with previous studies that have found that the superparamagnetic submicron sphere is normally composed of small nanoparticles that have a superparamagnetic property.

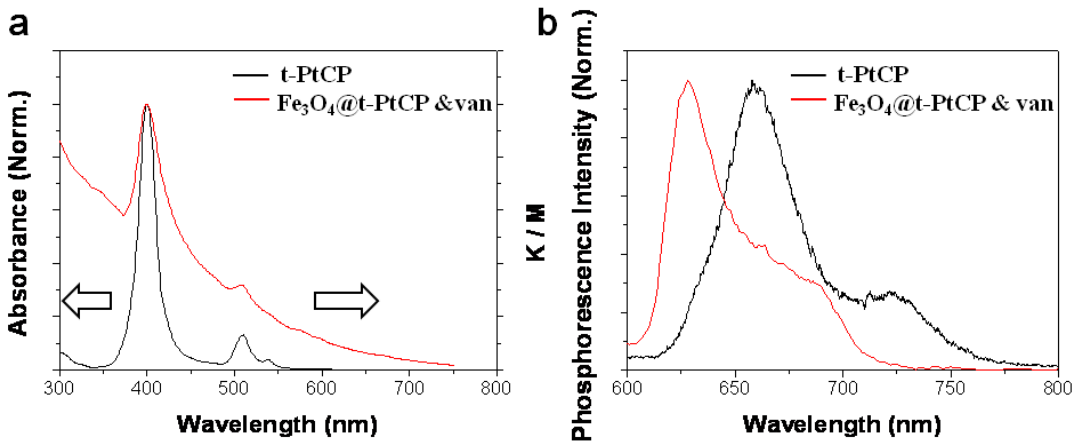

Fig. S4. (a) Absorption and (b) emission spectra of pure t-PtCP and the MMPs in THF. The absorption spectrum is obtained by applying the Kubelka-Munk function to the diffuse reflectance spectrum. The excitation wavelength is 510 nm for the emission spectrum.

Fig. S4 shows the difference between the absorption spectrum of t-PtCP in THF solution and the diffuse reflectance absorption spectrum of the MMPs suspended in THF solution. The Soret band at 400 nm and the Q bands located at 510 nm and 538 nm consistently appeared in two samples. At the excitation of 408 nm, the t-PtCP solution produces two strong emission peaks located at 660 and 725 nm, whereas the photofunctional magnetic submicron particles show the blue shifted peaks at 628 and 680 nm. Such blue shift also suggests that a strong coupling exists between t-PtCP and the surface of the magnetic particle.

The coverage amount of t-PtCP and vancomycin on particle

The concentration of t-PtCP molecules bonded to the surfaces of the magnetic particles was estimated by using UV-visible absorption spectroscopy. The comparative absorption ODs at 510 nm was measured with the reference t-PtCP solution (1.16×10^{-2} mM) before the insertion of the magnetic particles for reaction and the remaining t-PtCP solution obtained after the reaction with the particles. The O.D. difference indicates that ~ 1.16×10^{-7} mol (equivalent to 6.98×10^{16} molecules) of t-PtCP are immobilized onto the surface of 1 mg of magnetic particles. Assuming the density of the magnetic particles to be 5.15 g/cm^3,[3,17] 1 mg of the magnetic nanoparticles has the particle number of 6.26×10^9. Therefore, it leads to the estimation that the 1.1×10^7 t-PtCP molecules are approximately immobilized on the surface of each magnetic particle that has a diameter of 400nm. The concentration of VAN molecules bonded to the surfaces of the magnetic particles was estimated by the O.D. difference of the absorption peaks at 280 nm. The relative O.D. difference was estimated by a similar process as the above case of t-PtCP. O.D.s of the VAN solutions were measured with the initial solution before the reaction and the final solution after the reaction with the particles. The results shows that 5.05 μg of VAN are immobilized onto 1mg of Fe_3O_4@t-PtCP particles. 5.05 μg of VAN correspond to 3.48×10^{-9} mol (equivalent to 2.09×10^{15} molecules). Since 1mg of magnetic particles are equivalent to 6.26×10^9 particles,[3] $3.34\text{x}10^5$ molecules of VAN are approximately conjugated onto the surface of each Fe_3O_4@t-PtCP particles.

Detection capability of MMPs

The 6.26×10^9 particles (MMPs; vancomycin conjugated Fe_3O_4@t-PtCP particles) were used to capture 10^6 bacteria in the study. The MMPs bound to the surface of one bacterium cell were approximately estimated by calculating the surface volumes of each bacterium and MMPs. The MMPs is a spherical shape of 400 nm diameter and most bacteria is also spherical shape of 1 μm diameter. The surface area of one bacterium is 3.14×10^6 nm^2 and the cross-sectional area of each particle is 1.26×10^5 nm^2. As an approximated result, the 2.5×10^1 MMPs (diameter of 400 nm) are estimated to be bounded to the surface of one bacterium (diameter of 1 μm). Therefore 2.50×10^7 MMPs are required to capture the 10^6 bacteria. So, the optimum number of MMPs is 2.50×10^7 MMPs for capturing of 10^6 bacteria. The used particle number in the study is 6.26×10^9 which are excessive amount by approximately 250 times. Therefore the particles amount used in the study provides the full coverage for 10^6 bacteria and Fig. S5 that presents many magnetic particles adsorbed to a bacterium may suggest that very low detection limit can be expected with this multifunctional magnetic particle system.

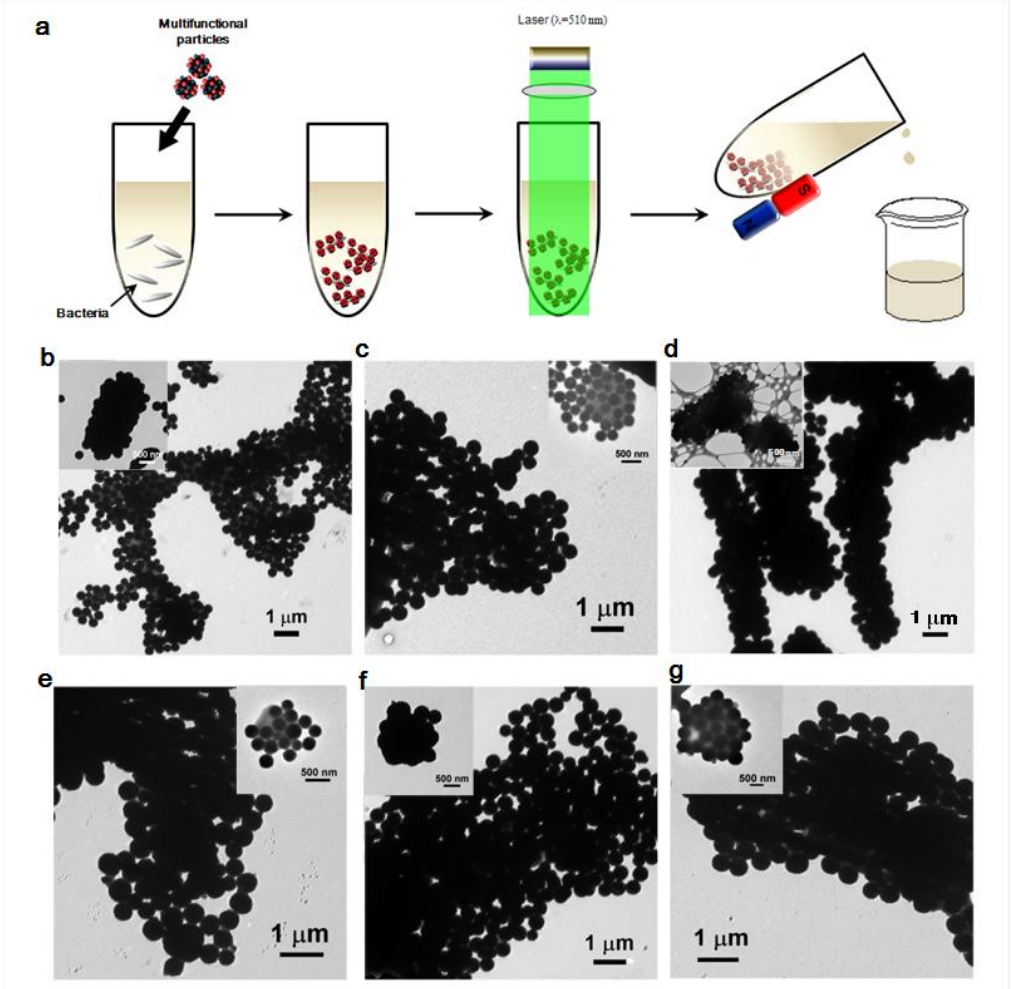

Fig. S5. (a) A schematic for the capture and killing of bacteria using MMPs and the confirmation of viability after laser irradiation. TEM images of (b) *S. typhimurium*, (c) *E. faecalis*, (d) *B. cereus*, (e) MSSA, (f) MRSA, and (g) VRE; these images were obtained with the bacteria that were incubated with the MMPs and isolated magnetically. Insets show the TEM images that represent a single cell of each bacterium.

Fig. S5 shows a schematic diagram for capturing bacteria with the use of MMPs and the confirmation of bacteria death following light irradiation. As the MMPs are added to the bacterial solution (10^6 CFU/mL), bacteria are captured by the MMPs due to the binding ability of VAN against the bacteria cell wall. The bacteria-captured multifunctional particle

complexes are separated from the uncaptured bacteria using a magnet. TEM images for the capture fractions of bacteria and MMPs were taken (Fig. 5b-f). The cell walls of the bacteria appeared to be fully covered by the MMPs. This clearly indicates that the MMPs were capable of recognizing and binding to the cell walls of Gram-positive and Gram-negative bacteria.

Table S1. Capturing capacity of MMPs and the bactericidal effect of MMPs without irradiation and Fe_3O_4@van particles with irradiation.

Bacterial strain	Survival fraction N_c/N_i* [%]				
	Fe_3O_4@t-PtCP	Fe_3O_4@t-PtCP&van (MMPs)		Fe_3O_4@van	
	Capturing capacity	Capturing capacity	Bactericidal effect after 12h incubation without irradiation	Capturing capacity	Bactericidal effect after laser irradiation
S. aureus	0.39 ± 0.06 % (4.75×10^3)	83.06 ± 5.48 % (1.30×10^6)	84.29 ± 4.25 % (1.32×10^6)	84.80 ± 4.17 % (1.11×10^6)	85.18 ± 1.03 % (1.12×10^6)
E. faecalis	0.38 ± 0.01 % (4.10×10^3)	88.29 ± 2.96 % (2.07×10^6)	86.01 ± 1.28 % (2.02×10^6)	88.37 ± 4.13 % (1.69×10^6)	87.31 ± 1.44 % (1.67×10^6)
B. cereus	0.34 ± 0.08 % (3.85×10^3)	86.27 ± 1.23 % (9.80×10^5)	86.01 ± 1.84 % (9.75×10^5)	89.29 ± 2.38 % (1.02×10^6)	87.11 ± 2.06 % (9.90×10^6)
MSSA	0.36 ± 0.02 % (5.55×10^3)	83.85 ± 4.94 % (1.35×10^6)	83.01 ± 3.92 % (1.27×10^6)	85.39 ± 0.55 % (1.31×10^6)	85.46 ± 0.03 % (1.31×10^6)
MRSA	0.38 ± 0.02 % (5.70×10^3)	84.11 ± 2.79 % (1.35×10^6)	85.64 ± 1.88 % (1.28×10^6)	84.90 ± 1.68 % (1.27×10^6)	85.34 ± 3.26 % (1.27×10^6)
VRE	0.38 ± 0.01 % (7.00×10^3)	84.87 ± 0.41 % (2.02×10^6)	84.84 ± 2.04 % (1.58×10^6)	86.18 ± 0.27 % (1.60×10^6)	86.26 ± 0.56 % (1.60×10^6)
***E. coli* O157**:H7:K^-	0.38 ± 0.03 % (5.00×10^3)	47.90 ± 0.53 % (4.79×10^5)	47.41 ± 1.02 % (4.74×10^5)	49.39 ± 9.62 % (5.36×10^5)	50.24 ± 0.74 % (5.46×10^5)
S. typhimurium	0.53 ± 0.03 % (6.20×10^3)	49.05 ± 3.57 % (4.90×10^5)	48.73 ± 3.88 % (4.87×10^5)	47.75 ± 0.50 % (5.83×10^5)	46.92 2.03 % (5.73×10^5)

* N_c = number of conjugated bacterial cells to particles, N_i = number of input bacterial cells

To determine the bacteria-capturing capacity of MMPs, 10^6 CFU/mL of eight bacteria, *E. faecalis*, *S. aureus*, *B. cereus*, MSSA, MRSA, VRE, *E. coli* O157:H7:K^-, and *S. typhimurium* were mixed with the MMPs for 2 h, respectively. From the mixed solutions, each of the bacteria-captured particle complexes were separated using a magnet to calculate the number of captured bacteria. As shown in Table S1, the bacteria capture capacity of the Fe_3O_4@t-PtCP particles was 0.40 ± 0.01 % of the original number of bacteria. This poor capture fraction is ascribed to the nonspecific binding between the particles and the bacteria (first column of Table S1). However, in the case of the MMPs, the bacteria capture capacity was

84.84 ± 1.70 % for Gram-positive bacteria and 48.48 ± 1.79 % for Gram-negative bacteria (second column of Table S1).

The bactericidal effects of VAN, PS (t-PtCP), and laser irradiation were also investigated as follows. The MMPs were mixed with seven types of bacteria for the toxicity test of VAN. To prevent the bactericidal effects caused by the generated $^1O_2$ from the photoexcited PS, the samples were prepared and incubated at room temperature for 12 h in complete darkness. The number of bacteria after 12 h of incubation was not reduced, indicating that the VAN bonded with bacteria did not affect the survival rate within 12 h (third column of Table S1). To examine the toxicity of t-PtCP, the captured bacteria with Fe_3O_4@van particles without t-PtCP were separated onto a BHI agar plate. There was no difference between the survival rates for the samples with and without t-PtCP, implying that t-PtCP itself was not toxic to the bacterial cells without light irradiation (fourth column of Table S1). Finally, to determine the effect of laser irradiation on survival rate, the capture fraction of the Fe_3O_4@van particles was irradiated with a laser at 510 nm with 6.1 mW/cm^2 of power density for 6 min for Gram-positive and 60 min for Gram-negative bacteria. The number of bacteria did not change, which meant that the laser irradiation itself did not kill the bacteria in the absence of t-PtCP (fifth column of Table S1).

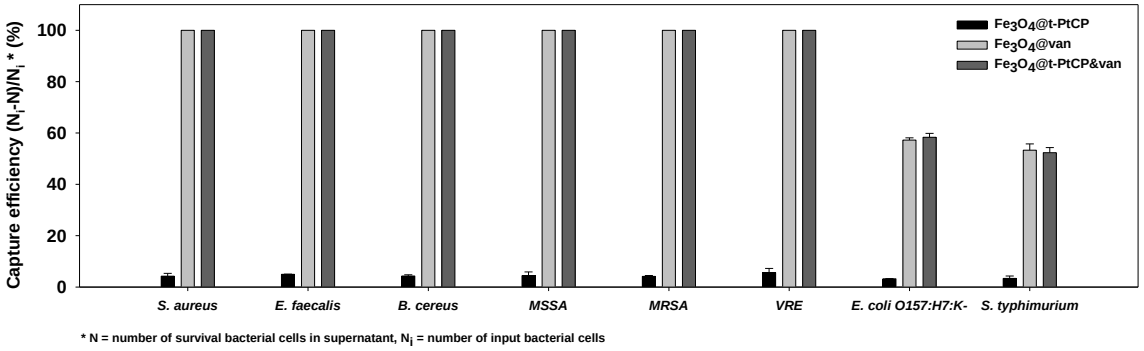

Fig. S6. Capture efficiency with supernatants following magnetic separation.

These capturing efficiencies were reconfirmed by checking the remaining bacteria in the supernatant after magnetic separation. No Gram-positive bacteria were detected in the supernatant, indicating that 100% of Gram-positive bacteria were captured by the MMPs. These results confirm that VAN is a very efficient molecule for binding the MMPs to the bacteria. Similar to previous reports, our study also confirms that although Gram-positive bacteria are completely captured by VAN, this is not the case for Gram-negative bacteria, which are not captured as efficiently.[11]

The difference between the capture efficiency estimated by the number of bacteria in the capture fraction compared with that in the supernatant seemed to originate from miscounting the aggregated bacteria in the capture fraction.[12] Indeed, the bacteria numbers were reduced by about 15% in the capture fraction compared with the capture efficiency estimated from the supernatant. As shown in the capture efficiencies of Fig. S2, VAN is more efficiently bound to Gram-positive than Gram-negative bacteria.[3] There is evidence that VAN effectively binds to a specific part (D-Ala-D-Ala moiety) of the cell wall called peptidoglycan.[13,14] However, peptidoglycan makes up only 5 ~ 20% of the cell wall in Gram-negative bacteria and is also hindered by an outer membrane.[15] VAN nevertheless captures various Gram-negative bacteria, albeit with lower efficiency, as reported in previous studies.[3,11,16]

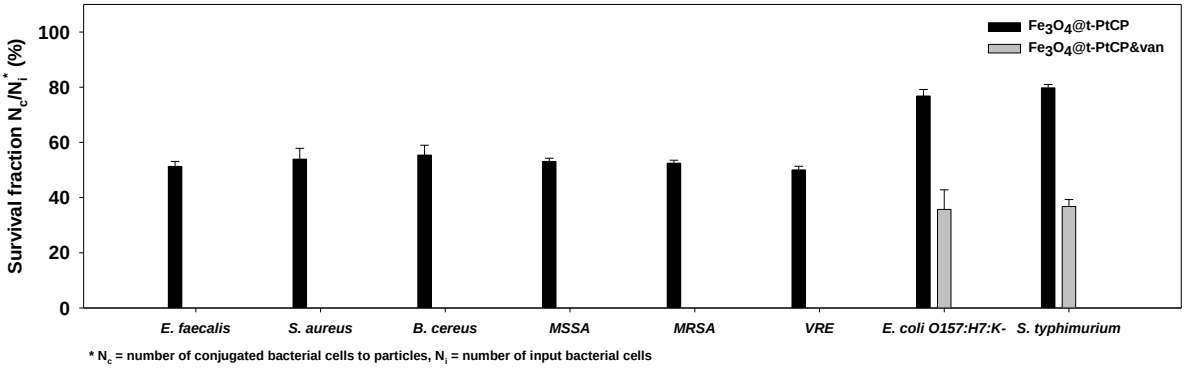

Fig. S7. Proximity effect on photodynamic inactivation by the VAN that is bonded to the MMPs. The experiments were performed with the capture fractions without magnetic separation. The bacteria except for E.Coli and S.typhimurium don't have any survival fraction with Fe_3O_4@t-PtCP&van under irradiation condition.

To confirm the proximity effect of the PS to the cell membrane, the same experiments as above were performed using the Fe_3O_4@t-PtCP particle without the bonded VAN. The result indicates that 47.84 ± 0.94 % of Gram-positive bacteria are killed after 6 min of laser irradiation, and less than 21.70 ± 1.33 % of Gram-negative bacteria are killed after 60 min irradiation. It presents a considerable difference in the efficiency of bacteria-killing, compared with the 100% (complete killing) and 63.75 ± 3.77 % killing of Gram-positive and Gram-negative bacteria with MMPs without the magnetic separation (Fig. S7). Therefore, the present study demonstrates that the close and selective proximity of PS to the bacteria surface is highly critical for the complete killing of bacteria, and such close contact can be achieved by using VAN as a targeting and capturing molecule.

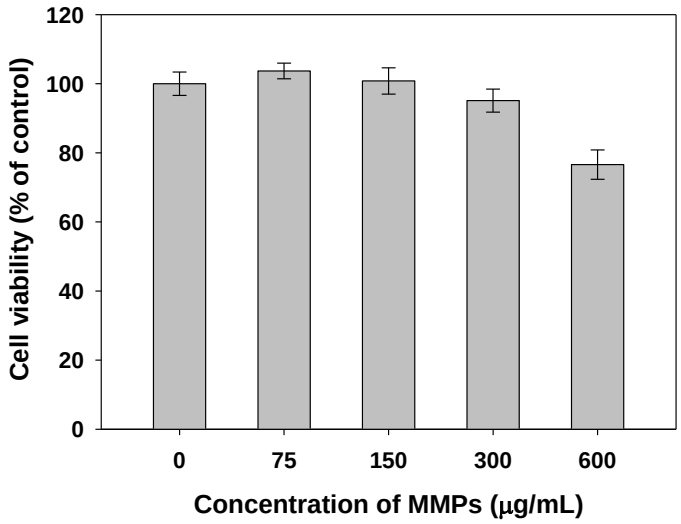

Fig. S8. Cytotoxicity of MMPs itself to L-929 cells incubated with various concentrations of MMPs for 24 hrs at 37°C in the dark.

Generally, the main goal of cytotoxicity testing is to assess the biocompatibility of biomaterial itself using mammalian cell culture system, because the test is useful in evaluating the toxicity of biomaterials and it provides a good way to screen biomaterials prior to *in vivo* tests. Therefore, newly fabricated biomaterial itself including degradable and non-degradable material is required to be evaluated for cytotoxicity regardless of the material functionality. Unlike other studies utilized in biological safety testing, cytotoxicity is not a pass/fail test. Therefore, we have tested the cytotoxicity of MMPs itself on L-929 cells using MTT assay according to the document of International standard (ISO 10993-5). This assay was used to assess the cell viability after exposure to MMPs at various concentrations (0, 75, 150, 300, 600 μg/mL) for 24 hrs. The results show Fig. S8. The data indicate no cytotoxicity of MMPs itself in the concentration range of 0 - 300 μg/mL, which are utilized for the photodynamic killing of bacteria in this study, in comparison with control. Cell viabilities are more than 95%.

References

1. H. Deng, X. L. Li, Q. Peng, X. Wang, J. P. Chen and Y. D. Li, *Angew. Chem. Int. Ed*. 2005, **44**, 2782-2785.
2. K. H. Choi, K. K. Wang, E. P. Shin, S. L. Oh, J. S. Jung and Y. R. Kim, *J Phys Chem* C 2011, **115**, 3212-3219.
3. Y. S. Lin, P. J. Tsai, M. F. Weng and Y. C. Chen, *Anal. Chem.* 2005, **77**, 1753-1760.
4. J. H. Ha, S. Ko, C. H. Lee, W. Y. Lee and Y. R. Kim, *Chem Phys Lett*, 2001, **349**, 271-278.
5. P. R. Ogilby, *Chem Soc Rev*, 2010, **39**, 3181-3209.
6. M. Tsushima, K. Tokuda and T. Ohsaka, *Anal. Chem* 1994, **66**, 4551-4556.
7. M. A. J. Rodgers and P. T. Snowden, *J. Am. Chem. Soc.* 1982, **104**, 5541-5543.
8. International Standard ISO 10993-5 2009 Part 5: Tests for in vitro cytotoxicity., Switzerland: International Organization for Standardization.
9. P. Trivedi and D. Vasudevan, *Environ. Sci. Technol.* 2007, **41**, 3153-3158.
10. N. Q. Wu, L. Fu, M. Su, M. Aslam, K. C. Wong and V. P. Dravid, *Nano Lett.* 2004, **4**, 383-386.
11. A. J. Kell, G. Stewart, S. Ryan, R. Peytavi, M. Boissinot, A. Huletsky, M. G. Bergeron and B. Simard, *Acs Nano*, 2008, **2**, 1777-1788.
12. W. C. Huang, P. J. Tsai and Y. C. Chen, *Small*, 2009, **5**, 51-56.
13. J. H. Rao, J. Lahiri, L. Isaacs, R. M. Weis and G. M. Whitesides, *Science*, 1998, **280**, 708-711.
14. Z. Malik, H. Ladan, Y. Nitzan and B. Ehrenberg, *J. Photochem. Photobiol. B, Biol.* 1990, **6**, 419-430.
15. A. P. Kuzin, T. Sun, J. Jorczak-Baillass, V. L. Healy, C. T. Walsh and J. R. Knox, *Structure with Folding & Design*, 2000, **8**, 463-470.
16. H. W. Gu, P. L. Ho, K. W. T. Tsang, C. W. Yu and B. Xu, *Chem. Commun*. 2003, 1966-1967.
17. D. Ciprari, K. Jacob, R. Tannenbaum, *Macromolecules* 2006, **39**, 6565–6573.